Superconducting Carbides

DOI: 10.1002/anie.200904956

Superconductivity in Quasi One-Dimensional Carbides**

Wolfgang Scherer, Christoph Hauf, Manuel Presnitz, Ernst-Wilhelm Scheidt, Georg Eickerling,* Volker Eyert, Rolf-Dieter Hoffmann, Ute C. Rodewald, Adrienne Hammerschmidt, Christian Vogt, and Rainer Pöttgen**

Dedicated to Professor Hubert Schmidbaur on the occasion of his 75th birthday

Rare-earth (*RE*) transition-metal (T) carbides $RE_xT_yC_z$ have been intensively studied during the last thirty years with respect to their interesting crystal chemistry.[1–5] Since the pioneering theoretical studies by Burdett, Whangbo, and Hoffmann on YCoC (Figure 1 a) these species are considered as organometallic $[T_yC_z]^{\delta-}$ polyanions embedded in an ionic matrix provided by the rare-earth-metal atoms.[5] Within the zero-, one-, two, or three-dimensional polyanionic networks, the carbon atoms can be isolated (carbometallates[2,3]) or they can form C_2 pairs[1] or C_3 units.[6]

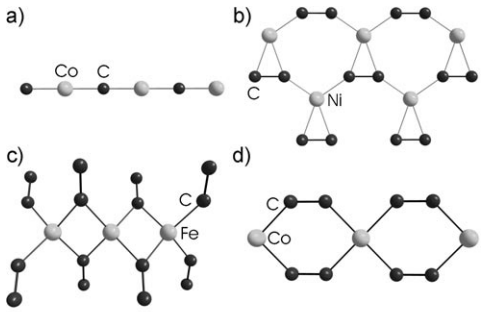

Figure 1. Structural models of the $[T_yC_z]^{\delta-}$ polyanions in a) YCoC, b) $LaNiC_2$, c) Y_2FeC_4, and d) Sc_3CoC_4.

Today, the $RE_xT_yC_z$ carbides are again the focus of intense research owing to their unprecedented physical properties. For example, the carbometallate YCoC which is the prototype of a low-dimensional $RE_xT_yC_z$ carbide, forms infinite linear -Co-C-Co-C- chains (Figure 1 a) and is characterized by its unusual high electronic heat capacity (Sommerfeld coefficient of $14.0\,mJ\,K^{-2}mol^{-1}$) suggesting the presence of narrow conduction bands.[7] The ternary nickel carbides $RENiC_2$ in particular, exhibit a variety of magnetic-ordering scenarios which depend on the nature of the rare-earth metal.[8a,b] However, the most prominent representative of this compound family is the noncentrosymmetric unconventional superconductor $LaNiC_2$ ($T_c = 2.7$ K; Figure 1 b).[8c–f] Superconductivity has been also observed in Y_2FeC_4 ($T_c = 3.6$ K) which has quasi one-dimensional $[FeC_4]$ moieties with iron in a distorted tetrahedral coordination environment (Figure 1 c).[9a] We note, that the superconductors $LaNiC_2$ and Y_2FeC_4 both have dicarbido C_2 moieties as common structural features. This observation supports the idea that the presence of antibonding π*(C–C) states near the Fermi level (which are absent in the carbometallate YCoC) might provide a prerequisite for the onset of superconductivity in the $RE_xT_yC_z$ carbides.[9b] The same argument also holds for the superconductivity in binary REC_2 carbides or the ternary $RE_2X_2C_2$ carbides (X = halogen).[9c] The absence of paramagnetic *RE* cations might be another criterion.

To identify further chemical control factors of the electronic-transport properties in covalent dicarbido compounds we analyzed the electronic structure of Sc_3TC_4 carbides (T = Fe (**1**), Co (**2**), Ni (**3**))[4,10] by experimental charge-density studies in combination with physical-property measurements down to ultra-low temperatures. The carbides **1**–**3** display quasi one-dimensional $[TC_4]$ ribbons with bridging μ-η^2-C_2 moieties (Figure 1 d). On the basis of topological analyses of the experimental charge densities of **1** and **2** we showed earlier that the bonding in the Sc_3TC_4 species is primarily controlled by covalent 1) σ(T←C) donation, 2) T→π*(C-C) back donation, and 3) partially covalent Sc–(η^2-C_2) bonding.[4a] This situation is also true for the nickel compound (Figure 2) which shows characteristic bond-path topologies in line with the presence of covalent Ni–C bonds and C–C bonds displaying significant π-bonding character (Table 1 and Supporting Information).[10]

Analyses of the atomic charge suggest that all $[TC_4]^{\delta-}$ polyanions carry approximately the same negative charge ($\delta \approx 4$) in **1**–**3**. Accordingly, the dicarbido $(C_2)^{2-}$ moieties display an atomic charge of approximately −2 ($Q(C_2) = -1.98$ (**1**); −2.11 (**2**) and −2.04 (**3**)) while the transition-metal atoms appear to be only slightly oxidized ($Q(T) = +0.5$ (Fe), +0.27 (Co), +0.13 (Ni).[4a,10] Hence, the iron species **1** can thus be

[*] Prof. Dr. W. Scherer, Dipl.-Phys. C. Hauf, Dipl.-Phys. M. Presnitz, Dr. E.-W. Scheidt, Dr. G. Eickerling, Dr. V. Eyert
Institut für Physik, Universität Augsburg
86135 Augsburg (Germany)
Fax: (+49) 821-598-3227
E-mail: wolfgang.scherer@physik.uni-augsburg.de
georg.eickerling@physik.uni-augsburg.de
Dr. R.-D. Hoffmann, Dipl.-Ing. U. C. Rodewald, Dr. A. Hammerschmidt, Dr. C. Vogt, Prof. Dr. R. Pöttgen
Institut für Anorganische und Analytische Chemie
Universität Münster
Corrensstrasse 30, 48149 Münster (Germany)
Fax: (+49) 251-83-36002
E-mail: pottgen@uni-muenster.de

[**] This work was supported by the Deutsche Forschungsgemeinschaft (SPP1178).

Supporting information for this article is available on the WWW under http://dx.doi.org/10.1002/anie.200904956.

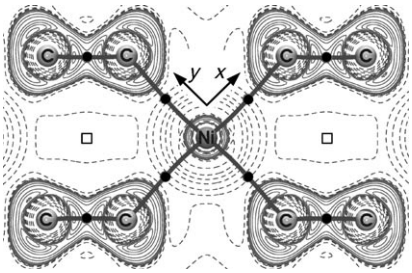

Figure 2. Experimental contour maps of the negative Laplacian of the charge density, $L(\mathbf{r}) = -\nabla^2\rho(\mathbf{r})$, in the plane defined by the $[Ni(C_2)_4]$ structural moiety of **3**; positive values (solid lines) and negative values (dashed lines); bond paths (solid lines), bond critical points (BCPs; closed black circles), and ring critical points (RCPs; open squares). Note, the definition of the local coordinate system and the transition-metal atom's crystallographic site symmetry as D_{2h}, which is close to D_{4h} if only the TC_4 moieties are considered.

Table 1: Comparison of the salient bond lengths of the $[TC_4]^{\delta-}$ moieties in **1**–**3** and the charge density, $\rho(\mathbf{r})_c$, at the respective bond critical points.[a]

	1 (T = Fe)	**2** (T = Co)	**3** (T = Ni)
T–C [Å]	2.1074(6)	2.0886(4)	2.094(1)
$\rho(\mathbf{r})_c$ [e Å^{-3}]	0.590 [0.553]	0.581 [0.572]	0.515 [0.563]
C-C [Å]	1.4498(11)	1.4539(8)	1.4561(13)
$\rho(\mathbf{r})_c$ [e Å^{-3}]	1.750 [1.765]	1.813 [1.769]	1.689 [1.746]
γ [mJ K^{-2} mol^{-1}][b]	17.0 [7.8]	5.7 [8.3]	7.7 [5.3]
$N_\gamma/N(E_F)$[c]	0.90 [0.42]	0.30 [0.44]	0.41 [0.28]

[a] The calculated values (DFT)[15] are based on the experimental geometries and are specified in square brackets (see ref. [12]). [b] The experimental Sommerfeld coefficient, γ, is based on specific heat measurements. [c] The theoretical DOS at the Fermi energy, $N(E_F)$, and the related experimental DOS, N_γ, are specified in [states/eV atom] (Supporting Information).

formally considered as 16 valence-electron (VE) species in which the Fe(d^8) center is coordinated by four $(C_2)^{2-}$ ligands in a square-planar manner. Accordingly, **2** and **3** represent 17 and 18 VE $[TC_4]^{\delta-}$ polyanions, respectively.

The close structural relationship of the isotypic carbides **1**–**3** is clearly reflected in their electronic structures. In earlier reports[4] we pointed out that the individual electronic bands of **1** and **2** show rather similar dispersions along selected symmetry lines within the first Brillouin zone of the body-centered orthorhombic unit cell; this is also true for **3**. Furthermore, the presence of the linear $[TC_4]$ ribbons is signaled in all three cases by reduced dispersions along the X–Γ and T–W lines (Figure 3a and Supporting Information). The major difference between the band structures of **1**–**3** is therefore mainly due to an increase of the d-electron count in the $[FeC_4]^{4-}$ (16 VE), $[CoC_4]^{4-}$ (17 VE), and $[NiC_4]^{4-}$ (18 VE) moieties and is responsible for the subsequent lifting of the Fermi level in the sequence **1**–**3**. Accordingly, the isotypic carbides **1**–**3** represent ideal model systems to study the electronic consequences of a stepwise population of higher energetic states—virtually decoupled from any pronounced differences in the chemical bonding in the $[TC_4]^{\delta-}$ polyanions (Table 1). The increasing electron count at the transition metal which subsequently leads to an increasing population of π*(C–C) states is reflected in a slight increase of the C–C distances in going from **1** to **3** (Table 1).[4a]

Major differences in the band structure of **1**–**3** are revealed by inspecting the site and state projected density of states (DOS) of the transition metal atom (Figure 3b,c and Supporting Information). Only the iron carbide **1** displays a sharp and large peak at the Fermi level ($N(E_F) = 0.42$ states/eV atom) which is due to Fe($d_{3z^2-r^2}$) states and a minor contribution from C(p_z) states. For symmetry reasons, these states represent basically nonbonding interactions in the $[FeC_4]$ ribbons of approximate local D_{4h} symmetry. The contributions of these states to the conduction band are, however, better revealed in the "fat band" representation of Figure 3a. In this case, the $d_{3z^2-r^2}$ state contribution is only dominant along the R–W and T–W lines, where the conduction band crossing the Fermi level is characterized by a rather weak dispersion—in line with the nonbonding character of these states. We suggested earlier[4a] that these localized $d_{3z^2-r^2}$ states in the reciprocal-space picture appear to be the origin of two axial valence-shell charge concentrations (denoted $VSCC_{ax}$ in Figure 4) at the iron atom. Note, that the cobalt carbide **2** as well as the nickel carbide **3** do not reveal any axial charge concentrations in the negative Laplacian maps, $L(\mathbf{r}) = -\nabla^2\rho(\mathbf{r})$, of the experimental charge-density distributions (Figure 4). This difference is due to the lack of localized $d_{3z^2-r^2}$ states at the Fermi level in **2** and **3** which is raised relative to that of the iron species.[4a,10] As a consequence the nature of the conduction bands in the cobalt and nickel species differ significantly from that of the iron species and display basically antibonding $T(d_{xz},d_{yz})/\pi^*(C–C)$ character (Figure 3c and Supporting Information).[4,12]

These differences should be also reflected in the physical properties of **1**–**3**. We therefore searched for additional experimental evidence to clarify whether a real-space property (local valence charge concentrations) might influence or

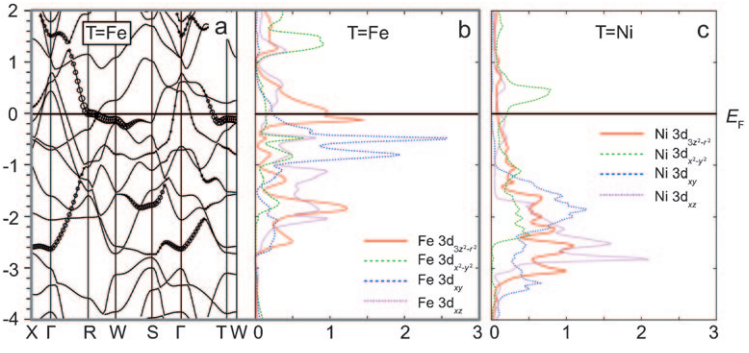

Figure 3. a) Electronic bands based on DFT calculations (see ref. [12]) of **1** (γ axis in eV) along selected symmetry lines within the first Brillouin zone of the body-centered orthorhombic unit cell. The radius of the circles given for each band weights the Fe($d_{3z^2-r^2}$) orbital contribution to the partial densities of states (DOS) at each *k* point. For a definition of the Brillouin zone and other relevant orbital contributions; see Supporting Information. b),c) Site and state projected partial DOS of **1** and **3** (in states/eV) in the energy range $E-E_F = -4$ to 2 eV. The position of the Fermi level (E_F) is indicated by a horizontal black line.

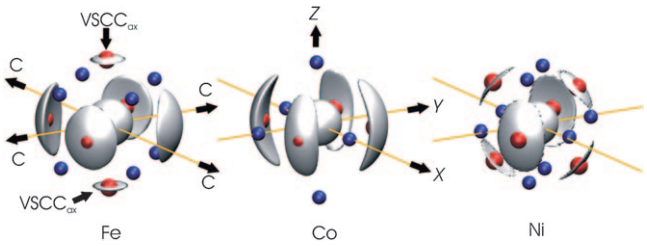

Figure 4. Experimental $L(\mathbf{r})$ envelope map of **1**, **2**, and **3**; $L(\mathbf{r}) = 777$, 1400, and 1301 eÅ^{-5}, respectively. The location of the local charge concentrations (red spheres) and depletions (blue spheres; (3, −3) and (3, +1) critical points) in the valence shell charge concentration (VSCC) of the transition metal atoms are shown. Note the additional charge concentrations (VSCC$_{ax}$) above and below the [TC$_4$] plane in the case of **1** which are absent in **2** and **3**.

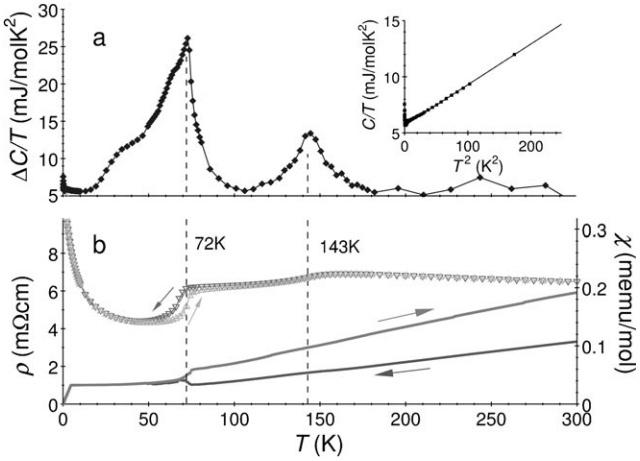

Figure 5. a) The temperature-dependent electronic contribution of the specific heat of **2**, ΔC, divided by temperature. b) The magnetic molar susceptibility, χ, at $B = 1$ T (triangles, right scale) and the electrical resistivity, ρ (solid lines, left scale). The arrows specify the cooling and warming sequences of the measurements. The dashed lines in (a) and (b) indicate the two anomalies at 72 K and 143 K. Inset: C/T versus T^2 plot from which the Sommerfeld coefficient γ was derived by a linear fit between 7 K and 14 K (solid line).

even control a reciprocal-space property (e.g. the electronic conductivity). Indeed, the presence of a narrow conduction band and the resulting high density of states is reflected by a high electronic heat capacity contribution in case of the iron carbide **1** (Sommerfeld coefficient $\gamma = 17.0\ \mathrm{mJ\,K^{-2}\,mol^{-1}}$;[14] Table 1). In contrast, the lack of a narrow conduction band (and axial VSCCs at the transition metal) might be correlated in **2** and **3** with their smaller Sommerfeld coefficients ($\gamma = 5.7$ and $7.7\ \mathrm{mJ\,K^{-2}\,mol^{-1}}$; Table 1). These findings provide strong experimental evidence for our earlier suggestion[4a] that the fine structure of the Laplacian pattern—in real space—can be employed as an electron-localization function in reciprocal space to trace the presence of narrow conduction bands in solids.

To our surprise, the cobalt carbide **2** can be discriminated from its nickel congener **3** by comparing their electronic conductivities, despite their similar γ values. Only the cobalt compound displays superconducting behavior below 4.5 K and a structural phase transition around 70 K. We therefore analyzed the physical properties of **2** in greater detail.

In Figure 5a the electronic contribution of the specific heat divided by temperature, $\Delta C/T$, of **2** reveals two distinct anomalies at 143 K and 72 K. These features were also observed in the temperature-dependent DC-susceptibility, $\chi(T)$, and the electrical resistivity, $\rho(T)$, (Figure 5b). The anomaly at 143 K is most likely due to a charge-density wave formation. The hysteretic behavior between the cooling and warming cycles in $\chi(T)$ and $\rho(T)$ at about 70 K, however, suggests a structural phase transition. Indeed, a single-crystal X-ray diffraction study at 9 K reveals the presence of a low-temperature (LT) modification of **2**, denoted LT-Sc_3CoC_4 in the following (Figure 6). Structural and charge-density analyses clearly reveal a Peierls-type distortion with alternating out-of-plane displacements of the cobalt atoms above and below the [CoC_4] ribbons. This displacement leads to alternating shorter (3.159 Å) and longer (3.601 Å) Co–Co distances between adjacent one-dimensional [CoC_4] ribbons.

The same type of structural distortion has been observed for the remaining Group 9 carbides Sc_3RhC_4 and Sc_3IrC_4.[16a] In case of the Group 8 and 10 carbides **1** and **3** we could, however, not find any evidence for such a structural phase transition above 2 K. This result might provide first evidence

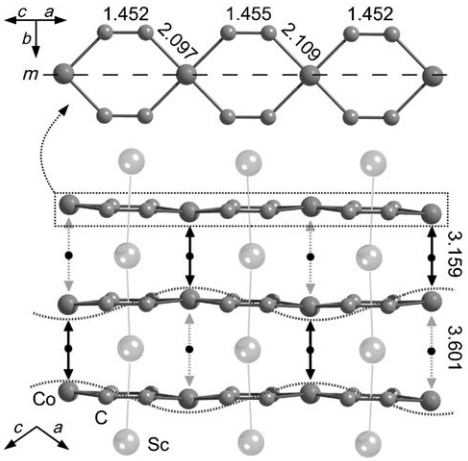

Figure 6. Structural model of LT-**2** illustrating the alternating out-of-plane distortions of the Co atoms in the [CoC_4] ribbons leading to [Co–Co···Co] chains with alternating short (gray arrows) and long (black arrows) Co–Co distances [Å]; *m* denotes the location of the crystallographic mirror plane in the transition-metal carbide moiety; the location of Co–Co bond critical points (BCPs) is depicted by black closed circles.

that the superconducting transition below 4.5 K in Sc_3CoC_4 critically depends on the presence of a Peierls-type transition along the transition-metal chains. This suggestion is further supported by the change in electrical resistivity of **2** on cooling (Figure 5b), which reveals a distinct increase of the $\rho(T)$ values below the structural transition temperature at 72 K.[16b] This change reflects a reduced electronic conductivity along the Co chains below the Peierls transition temperature. Such increasing electronic isolation of the quasi one-dimensional [CoC_4] ribbons is also in line with the increase of

$N(E_F)$ by 66% below the structural transition temperature of **2**. We further note, that symmetry reduction during the Peierls-type transition in **2** also has consequences with respect to the phonon spectrum. Hence, the out-of-plane distortion modes of the Co atoms (Figure 6) and the increase of the density of states might be the prerequisites for the establishment of superconductivity in the quasi one-dimensional Sc_3TC_4 carbides and explain the absence of the superconductivity in the iron and nickel species. Thus we tried to find more experimental evidence for the quasi one-dimensional behavior of **2** at ultra low temperatures.

Figure 7 summarizes the magnetic-susceptibility, electrical-resistivity, and specific-heat measurements of the cobalt carbide below 10 K. The onset of superconductivity is clearly marked by a sudden drop in the resistivity at 4.5 K, which is

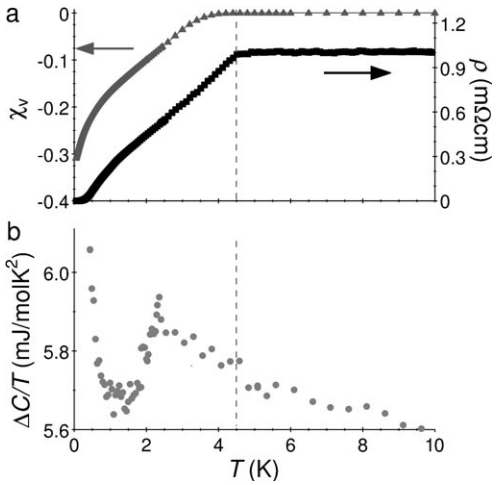

Figure 7. Temperature dependency of a) the volume susceptibility, χ_V at $B = 0.1$ mT, the electrical resistivity, ρ, and b) the electronic contribution of the specific heat divided by temperature $\Delta C/T$ of **2** below 10 K. The superconductivity begins below 4.5 K (broken vertical line).

accompanied by a diamagnetic response of the sample just below 4.5 K (Figure 7a). This result suggests that **2** can be classified as a bulk superconductor, since both, $\rho(T)$ as well as $\chi(T)$, simultaneously decrease below 4.5 K.[17] Also the large value of the volume susceptibility $\chi_V \approx -0.3$ at 50 mK and the specific heat anomaly (Figure 7b) provide further characteristic signatures of bulk superconductivity. The unusual shape of the specific-heat feature compared to a BCS-type superconductor (see for example, ref. [18]), however, may be characteristic for the presence of quasi one-dimensional $[CoC_4]^{\delta-}$ ribbons of **2**.[19] Hence, the quasi one-dimensional structural features and the unusual specific heat behavior might qualify **2** as one of the few model systems (e.g. poly(sulfur nitride) $(SN)_x$[20]) to study the chemical and physical prerequisites for the rare phenomenon of quasi one-dimensional superconductivity.

The isotypic Sc_3TC_4 carbides **1**–**3** are highly suitable benchmark systems because single crystals of excellent quality, suitable even for experimental charge density studies can be obtained. Careful inspection of the charge-density distribution in the valence shell of the transition metal atoms in **1**–**3** allowed differences in their electronic structures to be identified which is the key to understanding the quite different physical behavior of these otherwise electronically and structurally highly related systems.

Received: September 3, 2009
Revised: October 26, 2009
Published online: January 29, 2010

Keywords: band structure · electron density · solid-state structures · superconductors · transition-metal carbides

[1] W. Jeitschko, M. H. Gerss, R.-D. Hoffmann, St. Lee, *J. Less-Common Met.* **1989**, *156*, 397.
[2] a) A. O. Pecharskaya, E. P. Marusin, O. I. Bodak, M. D. Mazus, *Sov. Phys. Crystallogr.* **1990**, *35*, 25; b) G.-Y. Adachi, N. Imanaka, Z. Fuzhong in *Handbook on the Physics and Chemistry of Rare Earths*, *Vol. 15* (Eds.: K. A. Gschneidner, Jr., L. Eyring), Elsevier, Amsterdam, **1991**, chap. 69.
[3] E. Dashjav, G. Kreiner, W. Schnelle, F. R. Wagner, R. Kniep, W. Jeitschko, *J. Solid State Chem.* **2007**, *180*, 636.
[4] a) B. Rohrmoser, G. Eickerling, M. Presnitz, W. Scherer, V. Eyert, R.-D. Hoffmann, U. C. Rodewald, C. Vogt, R. Pöttgen, *J. Am. Chem. Soc.* **2007**, *129*, 9356; b) C. Vogt, R.-D. Hoffmann, U. C. Rodewald, G. Eickerling, M. Presnitz, V. Eyert, W. Scherer, R. Pöttgen, *Inorg. Chem.* **2009**, *48*, 6436.
[5] a) J. K. Burdett, *Prog. Solid State Chem.* **1984**, *15*, 173; b) M.-H. Whangbo in *Crystal Chemistry and Properties of Materials with Quasi-One-Dimensional Structures* (Ed.: J. Rouxel), Reidel, Dordrecht, **1986**, p. 27; c) R. Hoffmann, J. Li, R. A. Wheeler, *J. Am. Chem. Soc.* **1987**, *109*, 6600.
[6] a) R. Pöttgen, W. Jeitschko, *Inorg. Chem.* **1991**, *30*, 427; b) R. Pöttgen, W. Jeitschko, *Z. Naturforsch. B* **1992**, *47*, 358.
[7] a) K. Suzuki, T. Murayama, M. Eguchi, *J. Alloys Compd.* **2001**, *317–318*, 306; b) D. J. Singh, *Phys. Rev. B* **2002**, *66*, 132414.
[8] a) S. Shimomura, C. Hayashi, G. Asaka, N. Wakabayashi, M. Mizumaki, H. Onodera, *Phys. Rev. Lett.* **2009**, *102*, 076404; b) J. Laverock, T. D. Hynes, C. Utfeld, S. B. Dugdale, *Phys. Rev. B* **2009**, *80*, 125111; c) W. H. Lee, H. K. Zheng, *Solid State Commun.* **1997**, *101*, 323; d) W. H. Lee, H. K. Zheng, Y. Y. Chen, Y. D. Yao, J. C. Ho, *Solid State Commun.* **1997**, *102*, 433; e) A. D. Hillier, J. Quintanilla, R. Cywinski, *Phys. Rev. Lett.* **2009**, *102*, 117007; f) A. Subedi, D. J. Singh, *Phys. Rev. B* **2009**, *80*, 092506.
[9] a) M. H. Gerss, W. Jeitschko, L. Boonk, J. Nientiedt, J. Grobe, *J. Solid State Chem.* **1987**, *70*, 19; b) T. Gulden, W. Henn, O. Jepsen, R. K. Kremer, W. Schnelle, A. Simon, C. Felser, *Phys. Rev. B* **1997**, *56*, 9021; c) A. Simon, *Angew. Chem.* **1997**, *109*, 1873; *Angew. Chem. Int. Ed. Engl.* **1997**, *36*, 1788.
[10] a) Sc_3NiC_4 (**3**) was synthesized according to literature methods; see R.-D. Hoffmann, R. Pöttgen, W. Jeitschko, *J. Solid State Chem.* **1992**, *99*, 134, ref. [4a] (which also includes crystal data of **1** and **2** at 293(2) K) and the Supporting Information; Crystal data for **3**: $M_r = 241.61$, 293(2) K, $Mo_{K\alpha}$ radiation ($\lambda = 0.71073$ Å); black fragment, orthorhombic, space group *Immm*, $a = 3.4114(8)$, $b = 4.3911(8)$, $c = 11.923(3)$ Å, $V = 178.60(7)$ Å^3; $Z = 2$, $F(000) = 230$, $\rho_{calcd} = 4.49$ g cm^{-3}, $\mu = 10.4$ mm^{-1}. The data collection was carried out on an automated four-circle diffractometer (CAD4) equipped with a scintillation counter with pulse-height discrimination. A numerical absorption correction was then applied ($T_{min} = 0.423$, $T_{max} = 0.629$). The internal agreement factor was $R_{int}(F^2) = 0.0724$ for a total of 8364 reflections yielding 1018 unique reflections. This data set provided 100% completeness in $2 < 2\theta < 140$ ($\sin\theta_{max}/\lambda =$

1.322 Å^{-1}). The deformation density was described by a multipole model (Ref. [11a,b]) in terms of spherical harmonics multiplied by Slater-type radial functions (Ref. [11c]) with energy-optimized exponents (Ref. [11d]). The refinement of 42 parameters against 554 observed reflections [$F_o > 3\sigma(F)$, $\sin\theta_{max}/\lambda = 1.1$ Å^{-1}] converged to $R_1 = 0.0187$, $wR_2 = 0.0212$, and a featureless residual density map with minimum and maximum values of 0.38/−0.44 e Å^{-3}. For further information see Supporting Information. b) Crystal Data for LT-**2** at 9(2) K: $M_r = 241.85$, $Mo_{K\alpha}$ radiation (0.71073 Å); monoclinic, space group *C2/m* (Int. Tables No. 12), $a = 5.5375(6)$, $b = 12.030(2)$, $c = 5.5368(5)$ Å, $\beta = 104.77(1)°$, $V = 356.64(8)$ Å^3, $Z = 4$, 3028 reflections collected, 574 independent reflections [$R_{int} = 0.034$], $\mu = 9.798$ mm^{-1}, 42 parameters, goodness of fit 1.30, $R1(I > 2\sigma) = 0.049$, $wR2$(all data) = 0.129. For further information see the Supporting Information. CCDC 746186 (**3**, 293 K) and 752257 (**2**, 9 K) contain the supplementary crystallographic data for this paper. These data can be obtained free of charge from The Cambridge Crystallographic Data Centre via www.ccdc.cam.ac.uk/data_request/cif.

[11] a) N. K. Hansen, P. Coppens, *Acta Crystallogr. Sect. A* **1978**, *34*, 909; b) XD2006 (version 5.42)—a computer program for multipole refinement, topological analysis of charge densities and evaluation of intermolecular energies from experimental or theoretical structure factors; A. Volkov, P. Macchi, L. J. Farrugia, C. Gatti, P. Mallinson, T. Richter, T. Koritsanszky, **2006**; c) Z. Su, P. Coppens, *Acta Crystallogr. Sect. A* **1998**, *54*, 646; d) E. Clementi, D. L. Raimondi, *J. Chem. Phys.* **1963**, *38*, 2686.

[12] For analyses of the topology of theoretical charge-density distributions the *WIEN2k* and ASW programs were employed. The calculated charge densities were obtained using the gradient corrected density functional of Perdew, Burke and Ernzerhof (PBE). For the Wien2k calculations an augmented plane wave basis set with additional local orbitals (APW + lo) was employed; a) K. Schwarz, P. Blaha, G. Madsen, D. Kvasnicka, J. Luitz, *WIEN2k, An Augmented Plane Wave + Local Orbitals Program for Calculating Crystal Properties*, Technische Universität Wien, **2003**; b) V. Eyert, *The Augmented Spherical Wave Method—A Comprehensive Treatment*, *Lecture Notes in Physics 719*, Springer, Heidelberg, **2007**; c) J. P. Perdew, K. Burke, M. Ernzerhof, *Phys. Rev. Lett.* **1996**, *77*, 3865; d) J. P. Perdew, K. Burke, M. Ernzerhof, *Phys. Rev. Lett.* **1997**, *78*, 1396.

[13] We note, that spin-polarized DFT calculations predict a ferromagnetic ground state of **1** which is stabilized by 2.9 kJ mol^{-1} with respect to the value given by spin-averaged calculations. Taking into account the high density of states at the Fermi level this might hint for the presence of a weak-band ferromagnetic instability through the Stoner Mechanism as proposed for YCoC (see Ref. [7b]). This theoretical prediction is not supported by our magnetic measurements (1.7–400 K) yet and warrants further exploration by low-temperature studies.

[14] The Sommerfeld-coefficient γ has been derived from low-temperature specific-heat measurements. In the temperature range between 7 and 14 K **1**–**3** exhibit metallic behavior with $C/T = \gamma + \beta T^2$.

[15] In our DFT calculations employing the *WIEN2k* or the ASW program (see Supporting Information and ref. [12]) we find consistently significantly lower γ values for **1** in comparison with the experimental value derived from specific-heat measurements according to ref. [14].

[16] a) C. Vogt, R.-D. Hoffmann, R. Pöttgen, *Solid State Sci.* **2005**, *7*, 1003; b) The increase in the $\rho(T)$ values during heating above the structural phase transition is mainly caused by stress induced in the sample during the "translationsgleiche" phase transition of index *t2*, allowing twinning by pseudo-merohedry due to a change of the crystal system from orthorhombic to monoclinic. This is clearly monitored in our diffraction study by an additional splitting of the Bragg reflections.

[17] D. Saint-James, P. G. de Gennes, *Phys. Lett.* **1963**, *7*, 306.

[18] B. Mühlschlegel, *Z. Phys.* **1959**, *155*, 313.

[19] However, we note, that only (0.7 ± 0.05) mJ K^{-2} mol^{-1} of the total electronic specific heat $\gamma = 5.7$ mJ K^{-2} mol^{-1} contributes to the superconductivity in **2**. Therefore, the bulk superconductivity may be related solely to small areas of the Fermi surface.

[20] L. F. Lou, *J. Appl. Phys.* **1989**, *66*, 979.

